Journal of Modern Optics
Publication details, including instructions for authors and subscription information:
http://www.tandfonline.com/loi/tmop20

Nonlinear optical interactions of laser modes in quantum cascade lasers

Aleksander K. Wójcik [a], Nanfang Yu [b], Federico Capasso [b] & Alexey Belyanin [a]

[a] Department of Physics and Astronomy, Texas A&M University, College Station, TX 77843, USA

[b] School of Engineering and Applied Sciences, Harvard University, Cambridge, MA 02138, USA

Available online: 21 Apr 2011

To cite this article: Aleksander K. Wójcik, Nanfang Yu, Federico Capasso & Alexey Belyanin (2011): Nonlinear optical interactions of laser modes in quantum cascade lasers, Journal of Modern Optics, 58:9, 727-742

To link to this article: http://dx.doi.org/10.1080/09500340.2011.573590

Journal of Modern Optics
Vol. 58, No. 9, 20 May 2011, 727–742

Taylor & Francis
Taylor & Francis Group

INVITED TOPICAL REVIEW

Nonlinear optical interactions of laser modes in quantum cascade lasers

Aleksander K. Wójcik[a], Nanfang Yu[b], Federico Capasso[b] and Alexey Belyanin[a]*

[a]*Department of Physics and Astronomy, Texas A&M University, College Station, TX 77843, USA;*
[b]*School of Engineering and Applied Sciences, Harvard University, Cambridge, MA 02138, USA*

(*Received 1 January 2011; final version received 14 March 2011*)

We overview the results of recent experimental and theoretical studies of nonlinear dynamics of mid-infrared quantum cascade lasers (QCLs) associated with nonlinear interactions of laser modes. Particular attention is paid to phase-sensitive nonlinear mode mixing which turns out to be quite prominent in QCLs of different kinds and which gives rise to frequency and phase locking of laser modes. Nonlinear phase coupling of laser modes in QCLs leads to a variety of ultrafast and coherent phenomena: synchronization of transverse modes, beam steering, the RNGH multimode instability, and generation of mode-locked ultrashort pulses.

Keywords: quantum cascade lasers; nonlinear optics; mode locking

1. Introduction

Quantum cascade lasers (QCLs) have made extremely rapid progress and have reached a remarkably high level of maturity over the last decade. Mid-infrared QCLs were demonstrated to operate in the continuous wave regime at or above room temperature with multiwatt power output and increasingly high wall-plug efficiency [1–4]. Terahertz QCLs are operating at increasingly longer wavelengths reaching hundreds of micrometers [5,6]. As the devices become more mature, the time is getting ripe for in-depth studies of the nonlinear dynamics of laser modes in QCLs and its potential applications for multimode operation, nonlinear frequency mixing, frequency and phase coupling of laser modes, mode locking, pulsed operation, and frequency combs. The purpose of this paper is to review recent progress in this area and outline major challenges and prospects for future development.

Nonlinear dynamics of laser modes in QCLs has several peculiar features. Coupling of mid/far-infrared radiation with the active region in QCLs is extremely strong due to a large matrix element of the optical transitions between electron states in coupled quantum wells. This strong coupling, in combination with high intracavity laser intensity reaching several MW cm^{-2}, enhances a variety of nonlinear optical effects.

One universal nonlinearity inherently present in all kinds of lasers is the nonlinear saturation of the gain transition by laser modes which have inhomogeneous intensity distribution over the spectrum and over the spatial volume of the cavity. The inhomogeneous saturation leads to spectral and spatial hole burning, which, in turn, gives rise to multimode operation and nonlinear coupling between laser modes. This nonlinear coupling is phase sensitive and under certain conditions may lead to frequency and phase locking of laser modes. The latter process usually requires that some laser parameters, such as gain or losses, are periodically modulated, either externally or through the presence of some other nonlinear element in the cavity. It was recently shown [7–9] that phase locking of lateral modes in QCLs can be achieved spontaneously, due to the saturation nonlinearity of the gain transition alone. This effect turns out to be surprisingly robust; in many cases it leads to complete synchronization of lateral laser modes over a broad range of injection currents. The synchronization manifests itself as merging of combs of longitudinal modes into a singe equidistant comb and is accompanied by strong beam steering effects. This remarkable stability of the transverse mode locking is the consequence of another peculiar feature of QCLs: ultrafast gain recovery time of the order of 1 ps [10]. This timescale is much shorter than the cavity roundtrip time and the photon lifetime, which makes the QCL a class A laser [11], the only solid-state laser in this class. Ultrafast gain recovery time leads to overdamped relaxation oscillations, which stabilizes phase locking, as compared to class B lasers where phase locking of transverse modes is more difficult to achieve because of prominent relaxation oscillation resonance [12]. We overview recent results on the transverse mode locking in QCLs in Section 2.

*Corresponding author. Email: belyanin@tamu.edu

ISSN 0950–0340 print/ISSN 1362–3044 online

DOI: 10.1080/09500340.2011.573590
http://www.informaworld.com

Section 3 reviews recent work on the phase locking of longitudinal modes and generation of ultrashort pulses. The same mechanism which facilitates phase coupling of transverse modes, namely ultrafast gain relaxation, presents a fundamental obstacle for single-pulse operation in the mode-locked regime. Fast gain recovery damps any perturbation of light intensity in the cavity and prevents the formation of a stable pulse. In the modal language, the modes may be phase-locked, but they are locked to 'wrong' phases corresponding to a quasi-continuous wave output. Although in recent work [13] active mode locking by gain modulation in a short section of a QCL cavity has been demonstrated near laser threshold, passive mode locking remains an elusive goal. Still there is hope to achieve passive mode locking in the fully coherent regime when the timescale of Rabi oscillations of the population inversion and laser intensity becomes shorter than the dephasing time of the optical polarization; see [14–16]. Another possible avenue is to design lasers operating at the forbidden intersubband transition (e.g. diagonal in space) with very long relaxation time such as the device employed in [13].

2. Nonlinear coupling of transverse modes in QCLs

Recent studies [7–9] have shown that broad waveguide area QCLs capable of supporting several lateral modes often exhibit coherent effects in their modal dynamics, once a certain level of injection current has been reached. The intermodal coherence results from phase sensitive coupling of transverse modes through the inherent nonlinearity of gain saturation in the cavity. This can be observed as modal interference, which has as a consequence beam steering and asymmetry of the near field. The changes in the beam pattern occur and disappear suddenly, with a slight change of the injection current. These sudden changes in the beam shape are accompanied by changes in the laser spectrum. If the losses of the different transverse modes are similar, it is possible to achieve self-synchronisation of all the active modes in the cavity, with a constant phase relation between them.

Phase coupling of transverse laser modes has been extensively studied before, with the most recent surge of interest on this topic stimulated by applications in communications and optical information processing (chaos synchronization, control of pattern formation, spatial and polarization entanglement), see e.g. [17–20]. In all cases the synchronization was achieved by modulation of laser parameters, external optical feedback, or by coupling many lasers into laser arrays. QCLs seem to be unique, at least among solid-state lasers, in being able to maintain stable phase locking of transverse modes without any stabilizing elements, likely due to the combination of ultra-strong nonlinearity associated with intersubband laser transition and overdamped relaxation oscillations. When compared with other semiconductor lasers, their salient features and in particular the mechanisms of phase locking are quite different from the relevant properties of QCLs. In diode lasers, the locking is primarily due to density modulation of free carriers, which is proportional to the linewidth enhancement factor α. In QCLs the total electron density is not affected by the laser field and the α factor is much smaller. In this case the mode coupling is due to gain saturation across an intersubband atomic-like laser transition and the concomitant strong spatial hole burning, which favors multimode operation. Thus, studies of modal phase coherence in QCLs add a new dimension to this actively developing field and open up new potential applications in the mid-infrared and terahertz range, such as beam control and combining, electrical or optical switching/modulation, and free space communications; see e.g. [21–25].

The dynamics of the transverse modes can be described by a simple model that still captures the effect of phase-sensitive modal interactions.

First, we assume that the transverse and longitudinal dependence of the electromagnetic fields of the modes can be separated and the transverse dependence is further decomposed into the quasi-orthogonal waveguide modes of the 'cold' cavity:

$$\boldsymbol{E} = \sum_i e_i(t,z)\boldsymbol{E}_i(\boldsymbol{r}_\perp), \tag{1}$$

where $\boldsymbol{r}_\perp$ is the position vector in the cross-section of the waveguide and z is the coordinate along the cavity. The transverse distribution of the waveguide modes is calculated using COMSOL software for real device geometries used in experiments.

We introduce slowly varying complex amplitudes of the electric field:

$$e_i = \frac{1}{2}[a_i \exp(-\mathrm{i}\omega_0 t + \mathrm{i}\beta_i z) + \text{c.c.}], \tag{2}$$

where ω_0 is the laser transition frequency and β_i is the propagation constant of the ith mode. When needed, the plane wave dependence of the longitudinal modes can be replaced by a more realistic structure, counter-propagating modes are added, etc.

Next, we model the active region. Although the band structure of the laser involves multiple energy subbands and complex electronic transport (see for example [26,27]), for our purposes of studying the nonlinear dynamics of coupled modes the material gain

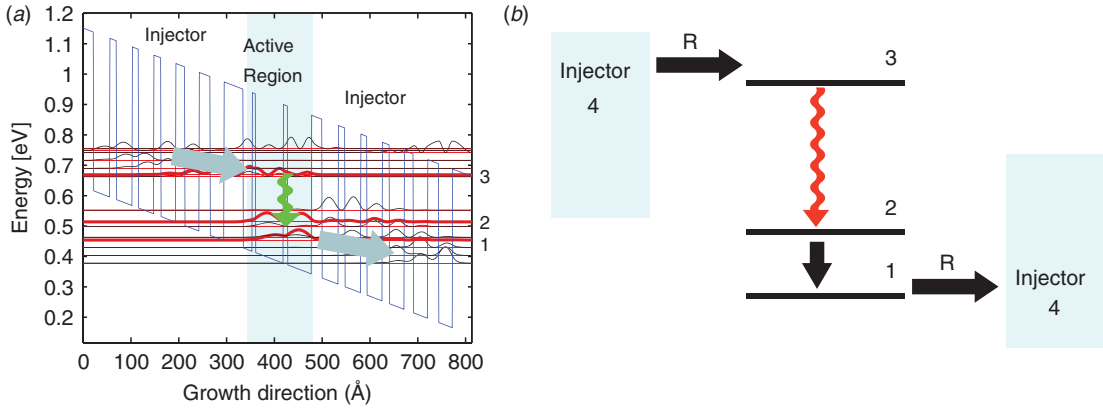

Figure 1. (*a*) Active region of one of the lasers used in mode locking studies reported in Section 3. The active region design follows the one described in [28]. (*b*) Its approximation by a four-level active laser medium. Bold arrows indicate electron transport due to LO phonon scattering and tunneling; wiggly arrow shows laser transition between states marked 3 and 2. (The color version of this figure is included in the online version of the journal.)

can be reduced to a two level medium, i.e. the standard Maxwell–Bloch equations.

Indeed, the electron flow through the typical active region of a QCL shown in Figure 1(*a*) can be roughly approximated by a four-level laser scheme as in Figure 1(*b*). The four-level scheme can be further reduced to the effective two-level scheme [11] if we take into account that the scattering time from lower laser state 2 to state 1 is very short (~0.2 ps) due to resonant LO-phonon emission. Therefore, state 2 stays almost empty and we can neglect its population. Then one can write the equation for the population inversion $D = N_3 - N_2$ between laser states 3 and 2 as shown in the second equation in Equations (4), where $T_1 = \gamma_\parallel^{-1}$ is the effective relaxation time for population inversion which can be expressed through the pumping rate R and scattering rates r_{31} and r_{32} from state 3 to states 2 and 1 as $\gamma_\parallel \simeq R + r_{31} + r_{32}$. The population inversion D_p supported by pumping in the absence of laser generation is given by $D_\mathrm{p} \simeq RN/(R + r_{31} + r_{32})$, where N is the total electron density in the active region. Note that in this approximation the population inversion D_p is always positive, even for an arbitrary small injection rate, and the value of D_p is proportional to the pumping rate R for small R.

The optical polarization is expressed through a slowly varying amplitude σ of the off-diagonal element of the density matrix as

$$P = Nd[\sigma \exp(-\mathrm{i}\omega_0 t) + \mathrm{c.c.}]. \tag{3}$$

By integrating Maxwell's equations over the cross-section A_T of the waveguide, making use of the quasi-orthogonality of the modes, and eliminating the fast oscillating terms (rotating wave approximation), we obtain

$$\begin{aligned}
\frac{\partial \sigma}{\partial t} + \gamma_\perp \sigma &= -\frac{\mathrm{i}d}{2\hbar} D \sum_i E_i a_i, \\
\frac{\partial D}{\partial t} + \gamma_\parallel (D - D_\mathrm{p}) &= -\frac{\mathrm{i}d}{\hbar} \sum_i (a_i^* \sigma - a_i \sigma^*), \\
\frac{\partial a_i}{\partial t} + \frac{c}{\mu_i}\frac{\partial a_i}{\partial z} + (\kappa_i + \mathrm{i}\Delta_{ci}) a_i &= \frac{4\pi \mathrm{i}\omega_0 N d}{\mu_i A_T} \int_{AR} \sigma E_i \, \mathrm{d}A,
\end{aligned} \tag{4}$$

where d is the dipole moment of the laser transition, $\Delta_{ci} = \omega_{ci} - \omega_0$ is the detuning of the ith mode from the central frequency ω_0, μ_i is the modal refractive index, and $T_2 = \gamma_\perp^{-1}$ is the relaxation time for the optical polarization.

We can simplify the equations further, by recognizing the extremely fast relaxation times of the polarization and population variables, which are enslaved by the field variables and can be eliminated adiabatically: $\mathrm{d}\sigma/\mathrm{d}t = 0$ and population $\mathrm{d}D/\mathrm{d}t = 0$ (class-A laser) [11]. We expand the polarization term in power series with respect to the field amplitudes and retain only the two lowest order terms (the $\chi^{(3)}$ approximation). The resulting equations of motion form a system of coupled nonlinear differential equations for the time dependent complex amplitudes of the modes. If necessary, the amplitude and phase fluctuations can be added phenomenologically.

The longitudinal structure corresponding to each of the transverse modes is conformed by a large number of longitudinal modes which can be averaged under a mean-field approximation. This is done by averaging the last equation over the z coordinate. All the losses,

including mirror and waveguide losses, are incorporated into the total modal losses κ_i. In this approximation the final form of the equation of motion for the ith mode becomes:

$$\frac{\mathrm{d}a_i}{\mathrm{d}t} + (\kappa_i + \mathrm{i}\Delta_{ci})a_i = g\Gamma_i a_i - \frac{g}{I_S}\sum_{j,k,l} a_j a_k^* a_l G_{ijkl}, \qquad (5)$$

where the material gain and saturation intensity are defined by

$$g = \frac{2\pi\omega_0 N d^2 D_p}{\gamma_\perp \hbar \mu_i}, \quad I_S = \frac{\hbar^2 \gamma_\parallel \gamma_\perp}{d^2}. \qquad (6)$$

Here the overlap integrals are defined as

$$\Gamma_i = \frac{\int_{AR} \varepsilon E_i^2 \,\mathrm{d}A}{\int_{A_T} \varepsilon E_i^2 \,\mathrm{d}A}, \quad O_i = \frac{1}{A_T}\int_{AR} \varepsilon E_i^2 \,\mathrm{d}A, \qquad (7)$$

$$G_{ijkl} = \frac{1}{A_T (O_i O_j O_k O_l)^{1/2}} \int_{AR} \varepsilon E_i E_j E_k E_l \,\mathrm{d}A, \qquad (8)$$

where AR is the cross-sectional area of the active region. The factors G_{ijkl} are symmetric with respect to any permutation of the sub-indices, which is clear from the definition, Equation (8). The symmetry simplifies the numerical calculations. The values of the factors G_{ijkl} depend on the device geometry and they can be of either sign.

The second term on the right-hand side of Equation (5) describes the phase-sensitive nonlinear coupling between different modes which can lead to their frequency and phase locking. This process competes with the effect of waveguide dispersion and losses described by the complex detunings (the second term on the left-hand side of Equation (5)).

As the final step we add phenomenologically a noise term to the equations. The class-A dynamics of QCLs modifies the noise analysis in this kind of laser from that of standard semiconductor lasers. The analysis can be further complicated by the correlation of photons through the reuse of electrons while they travel inside the cavity. The specifics of noise correlation effects are discussed in the literature [29,30].

In our analysis we concentrate on the simplified, phenomenological model of amplitude fluctuations, since it is this kind of noise that has the strongest effect on the modal stability [9]. The origin of these fluctuations is the stochastic nature of spontaneous emission. The effect on the modal dynamics of this noise is more important during the field build-up inside the cavity, during which the coherent amplitude and the noise are of the same order. Its importance decreases once the field amplitudes approach steady state. The importance of the fluctuations is more pronounced in bistable lasers, since the final state strongly depends on the initial conditions.

The noise enters our analysis as an extra equation, with a stochastic source term added to the complex field amplitude,

$$a_i(t) \to a_i(t) + \tilde{a}\xi_i(t). \qquad (9)$$

The noise term has the following characteristics:

$$\begin{aligned} \langle \xi_i(t) \rangle &= 0, \\ |\langle \xi_i(t)\xi_j(t') \rangle| &= \delta_{ij}\delta(t-t'). \end{aligned} \qquad (10)$$

Here $\tilde{a}$ is the noise amplitude and $\xi(t)$ is a stochastic process, with a complex uniform distribution function and $0 \le |\xi(t)| \le 1$.

Experiments with buried heterostructure QCLs show coherent interaction of the transverse modes. In our studies the observed near and far field patterns were fitted to three cavity modes. The relative intensities and phases of the modes change depending on the injection current, but a fixed set of transverse modes was used to explain the transverse behavior for any injection current.

Measurements of the near and far fields of a mid-infrared laser operating at a wavelength $\lambda \simeq 7.0\,\mu$m are presented in Figure 2, the width of the active region is 12.35 μm and is shown on Figure 2(*a*). The experiments were realized at room temperature in a pulsed mode operation with a repetition rate of 80 kHz. Far field and near field measurements were performed for a range of injection currents, with a fixed pulse duration of 125 ns. The same measurements were taken for different pulse durations, while maintaining a constant injection current of 1 A. Details of the setup and the NSOM apparatus used for the near field measurements can be found in [31].

The beam measurements from Figure 2(*c*), complemented by spectral measurements, show that the laser operates in three transverse modes. The modes TM_{00}, TM_{01} and TM_{02} were used to fit the near and far fields shown. The asymmetry of the laser profile can only be explained by the interference between modes. The coherent interaction of the modes persists over a wide range of injection currents. In wider active regions the phenomena was still observed, and the number of modes remained equal to three, but higher order modes were present [7].

Thermal effects can modify the refractive index and lead to distortion of the transverse field in QCLs [32]. In this case the asymmetry can be explained as a interference of two lowest order transverse modes [21]. In our experiments thermal effects can be observed for longer current pulse durations, which change the transverse beam shape, as is presented on Figure 2(*c*).

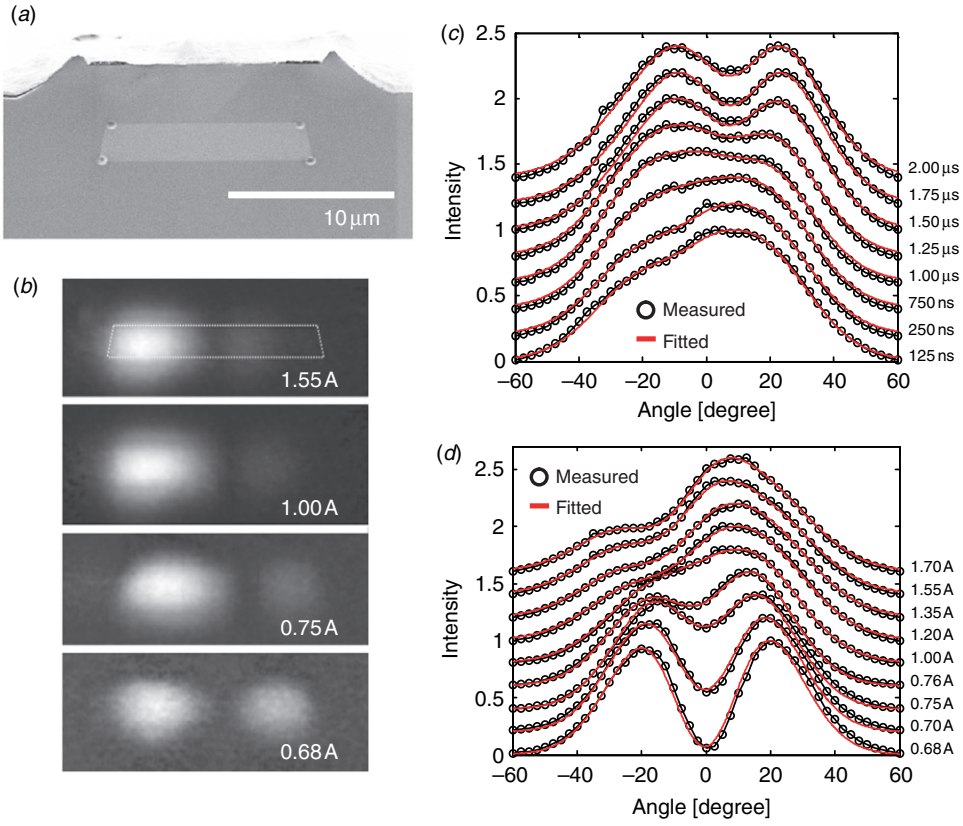

Figure 2. Near and far field measurements of a buried heterostructure QCL, with a repetition rate of 80 kHz. (*a*) The waveguide structure of the QCL. (*b*) Near field measurements with a 125 ns pulse duration and varying the injection current. (*c*) Pulse duration variation with a 1 A injection current. (*d*) Injection current variation with a 125 ns (1% duty cycle) pulse duration (from [7]). Reproduced with permission from Yu et al., Phys. Rev. Lett. 2009, 102, 013901. Copyright (2009) by the American Physical Society. (The color version of this figure is included in the online version of the journal.)

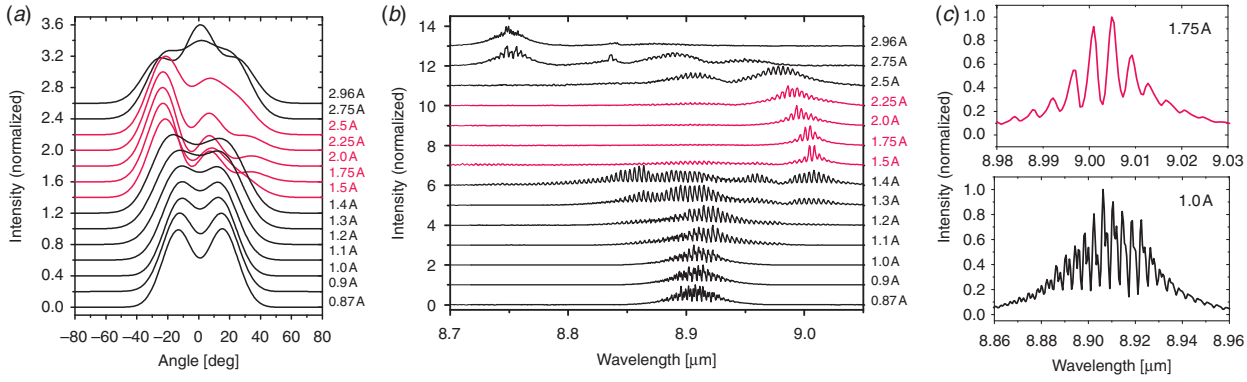

Figure 3. Laser measurements in the pulsed regime with different stability regions marked with different colors. (*a*) Far field measurements. (*b*) Spectra measurements. (*c*) A detail of the spectrum showing the merging of the combs of multiple transverse modes into a single comb, while the laser still operates in multi-transverse mode regime (from [8]). Reproduced with permission from Wójcik et al., Phys. Rev. Lett. 2011, 106, 133902. Copyright (2011) by the American Physical Society. (The color version of this figure is included in the online version of the journal.)

The observed asymmetry of the field disappears for longer pulse durations. The same effect can be observed at higher injection currents, including the roll over region, as seen in Figure 3. In terahertz QCLs, a different transverse effect was observed, the mode hopping between two modes through domain formation [24]. To distinguish between the regimes, a spectral analysis is necessary. In general a mixture of both effects can be expected, resulting in a combination of coherent and incoherent modal mixing.

The phases of the transverse modes presented in Figure 2 were correlated but their spectral combs remained distinct. An even more dramatic effect of the complete mode self-synchronization has been reported in [8]. In this case the complex spectrum of several distinct combs of longitudinal modes belonging to different transverse modes merges into a single comb while the laser maintains a multi-transverse mode operation. The transition to this regime occurs as a bifurcation at a certain value of the injection current. It is accompanied by the transition from the multi-stability regime where many stable steady-state solutions are possible to the regime where there exists only one stable steady state with phase coherence between lateral modes.

An experimental example of such a frequency- and phase-locked behavior is presented in Figure 3. The laser used is a buried-heterostructure laser fabricated by Hamamatsu, with an active region width of 19.4 μm. This is a high-performance laser based on three phonon resonance design as reported in [13,33]. It is operated at room temperature in a pulsed mode, with 125 ns pulse length and 80 kHz repetition rate. Starting from threshold, this laser shows three lateral modes: TM_{00}, TM_{01}, and TM_{02}, and its far field is well described by an incoherent addition of modal intensities. The spectrum consists of at least three distinct combs of longitudinal modes, each comb belonging to a different lateral mode. At about 1.5 A, both the spectrum and the far field undergo a drastic change. The spectral combs merge into a single comb (Figure 3(*b*)), as if only one lateral mode is present. Detailed analysis reveals three distinct RF peaks below the locking transition which correspond to the round-trip frequencies in three combs. Only one such peak exists above the locking transition. At the same time, the far field pattern becomes very asymmetric and shifts by about 30° off the waveguide axis (Figure 3(*a*)). This far field indicates the presence of all three lateral modes whose combs become completely synchronized. Again, we verified that the far field can only be fitted by a *coherent* addition of the fields of all three lateral modes with fixed mutual phases. Any incoherent addition of mode intensities cannot lead to the observed asymmetric distribution because all lateral modes are symmetric with respect to the waveguide axis.

The experimental results can be studied through numerical solution of the above modal equations of motion. The model allows one to study the transient effects, stability and steady state behavior of the modes and explain the observed experimental behavior. We studied the modal dynamics as a function of laser parameters: gain, losses, frequency detunings, etc. Two important limiting cases were analyzed: the single mode and the mean-field approximation. The mean-field approximation is presented first. In this approach the detuning variables represent the separation between adjacent transverse modes, while the longitudinal dependence is averaged out.

Before presenting numerical results we can derive simple analytic conditions for lateral mode locking [7]. Consider the four-wave mixing process of the type $TM_{01} + TM_{01} \leftrightarrow TM_{00} + TM_{02}$ relevant for the laser shown in Figure 2. Express the complex amplitude of the jth mode via its real amplitude and phase as $a_j(t) = f_j(t)\exp(i\phi_j(t) - i\Delta_j t)$, where $\Delta_j = \omega_j - \omega_0$ is the detuning of the frequency of a jth 'hot' mode from the transition frequency. Here 'hot' denotes actual (unknown) frequencies, phases, and amplitudes of laser modes with the nonlinear interaction taken into account. Then Equation (5) yields six equations with real coefficients for the amplitudes and phases of these modes. The phase difference corresponding to the above four-wave mixing process is

$$\begin{aligned} &\mathrm{d}(2\phi_2 - \phi_1 - \phi_3)/\mathrm{d}t + \delta_1 + \delta_3 - 2\delta_2 \\ &\quad = -(g/I_s)[(2f_1^2 + f_2^2)G_{1122}\sin 2\Phi_{12} + (2f_3^2 + f_2^2)G_{2233}\sin 2\Phi_{32} \\ &\qquad + (f_1^2 - f_3^2)G_{1133}\sin 2\Phi_{31} + 2f_2^2(f_1/f_3 - f_3/f_1)G_{1223}\sin\Phi_{31} \\ &\qquad - (4f_1f_3 + f_2^2(f_1/f_3 + f_3/f_1))G_{1223}\sin\Phi_{2231} \\ &\qquad + (f_1^2/f_3 - f_3)f_1G_{1113}\sin\Phi_{31} + (f_1 - f_3^2/f_1)f_3G_{1333}\sin\Phi_{31}], \end{aligned} \tag{11}$$

where indices 1, 2, and 3 correspond to modes TM_{00}, TM_{01}, and TM_{02}, respectively, $\delta_j = \omega_j - \omega_{cj}$, $\Phi_{jk} = \phi_j - \phi_k - (\omega_j - \omega_k)t$, and $\Phi_{2231} = 2\phi_2 - \phi_1 - \phi_3 - (2\omega_2 - \omega_1 - \omega_3)t$.

From Equation (11) we see that there are two possibilities to achieve phase locking $\mathrm{d}(2\phi_2 - \phi_1 - \phi_3)/\mathrm{d}t = 0$. The first situation is when $\omega_1 = \omega_2 = \omega_3$, i.e. three combs belonging to different lateral modes merge into a single comb. In this case the modal amplitudes f_j can be arbitrary as long as they correspond to a steady state. The second possibility is when the frequencies of the 'hot' modes are distinct but are locked to the relation $\omega_1 + \omega_3 = 2\omega_2$. In this case the modal amplitudes must satisfy the relation $f_1 = f_3$ whereas the amplitude of the mode 2 (TM_{01} mode) can be arbitrary. In both cases, the modal amplitudes have to be sufficiently large so that the nonlinear term on the right-hand side of Equation (5) cancels the term with complex detunings on the left-hand side originating from the waveguide dispersion of the 'cold' modes. These conditions qualitatively agree with the observed behavior of the amplitudes, phases, and frequencies of the lateral modes reported in [7–9].

The stability of the lateral mode locking can be analyzed by linearizing the phase difference in Equation (11) with respect to the phase-locked

steady state. There is a well known result [11] which says that the saturation nonlinearity of the inverted medium cannot give rise to a stable mode locking of longitudinal modes belonging to single transverse mode: the time derivative of the perturbation of the phase difference in Equation (11) is always positive. To achieve stable mode locking one has to add interaction with an absorbing medium (a saturable absorber). However, this result is no longer valid when the interacting longitudinal modes belong to different transverse modes. This is clear from the structure of Equation (11) where the factors G_{ijkl} on the right-hand side can be of either sign and the overall sign of the time derivative of the perturbation can be negative even if there is no nonlinear element in the cavity other than the nonlinearity of the gain transition.

We solve the system of coupled nonlinear differential equations (5) using Matlab. The initial conditions for the amplitudes are taken as a set of randomly distributed complex amplitudes, with magnitudes of the order of 10^{-3} in CGS units. This accounts for the amplification of the cold cavity modes from spontaneous emission. The equations are integrated until the amplitudes reach either steady state or a periodic form. We focus on the dynamics of three transverse modes, which has been the number of modes observed in the coherent coupling experiments. The transverse distributions, losses, frequencies, and propagation constants of cold waveguide modes were found with COMSOL software using the Finite Element Method and were consequently used to find the overlap integrals G and Γ.

An example of such analysis is shown in Figure 4(a) for the magnitudes of the complex amplitudes a_i. The nonlinear interaction leads to frequency pulling, merging the transverse modes into a single frequency with a constant phase difference between them. This can be observed from Figure 4(b), where the frequency is the slope of the phase. Experimentally this effect corresponds to the merging of three combs belonging to different transverse modes into a single comb, while the far field pattern shows the presence of all three transverse modes with locked phases. This is in good agreement with the results presented in Figure 3(c). The phase difference between the modes determines the exact form and the amount of the beam steering in the far field.

Now we make an assumption which is in a sense opposite to the mean-field approximation adopted above. We assume that the longitudinal dependence of the electric field corresponds to the standing wave modes in a cold lossless cavity, $\propto \sin(N_i \pi z/L_c)$, where L_c is the cavity length and N_i is an integer number of the order of ~1800 for our lasers. This approximation neglects any z-dependence of modal amplitudes and

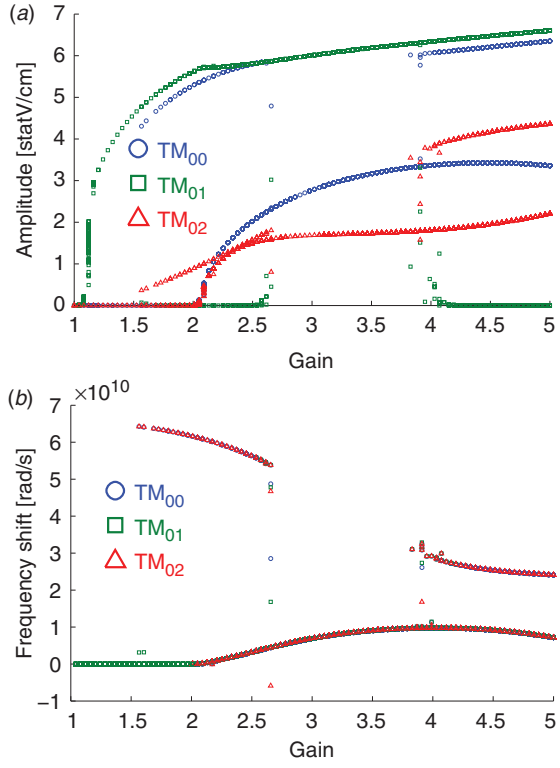

Figure 4. (a) Bistability in modal amplitudes as a function of gain, normalized to g_{th}. (b) Frequencies of all three modes lock to two different frequencies, normalized to g_{th} (from [9]). Reproduced with permission from Wójcik et al., Opt. Eng. 2010, 49, 111114. Copyright (2010) by SPIE. (The color version of this figure is included in the online version of the journal.)

carrier diffusion along z. The equations for the complex amplitudes Equations (5) remain of the same form, only the modal index i becomes a double index counting both transverse and longitudinal modes. Also, the overlap integrals G_{ijkl} now have to be taken over the cavity volume. These integrals contain the product of four sines with different arguments, so they are non-zero only for certain values of the longitudinal indices N_i.

One example of spectral location of frequencies of cold cavity modes is schematically shown in Figure 5(a). The spectrum can be split into the triplets where each triplet consists of longitudinal modes that belong to different lateral modes and have different longitudinal indices. The separation between the modes within each triplet is determined by the geometry of the cavity. Various cases of the mode alignment were explored with spectrally resolved near-field measurements in [34]. The lateral modes interact most efficiently when the overlap integral corresponding to the four-wave mixing process within each triplet is non-zero. Even in this case the interaction is weaker

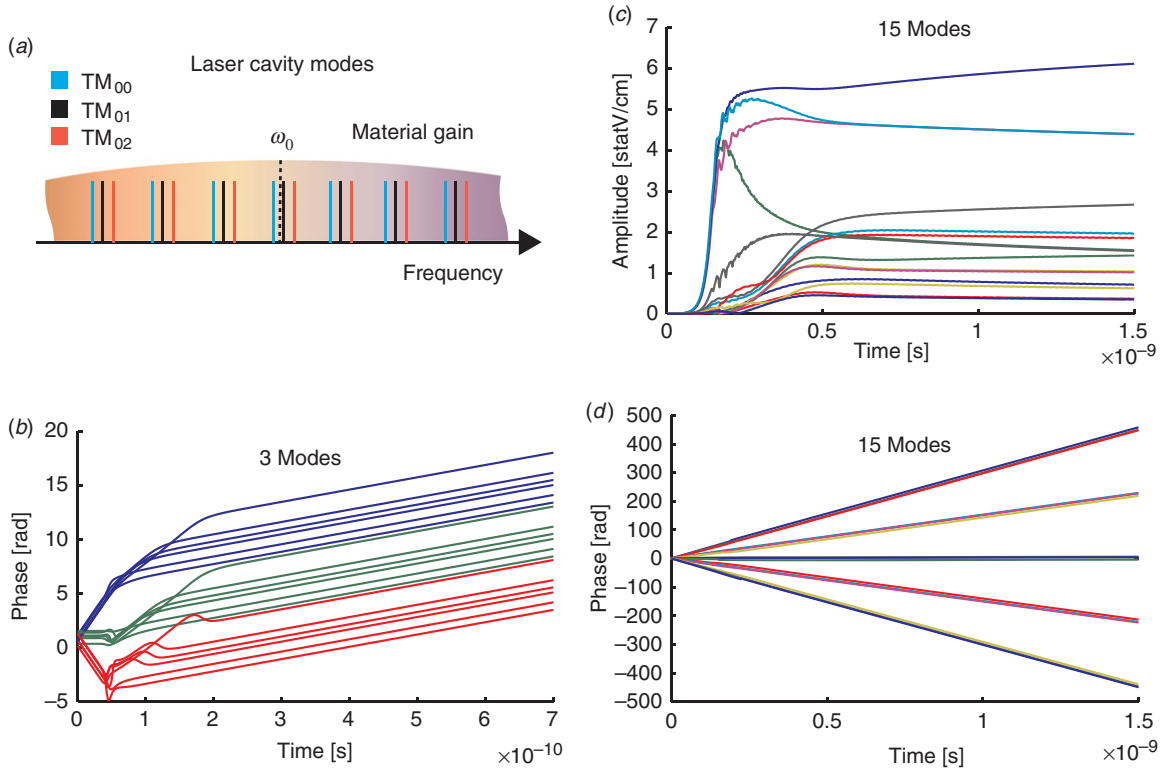

Figure 5. Time-dependent simulations of frequency and phase locking between lateral combs at the current three times the threshold current. (*a*) Schematic of spectral positions of cold cavity modes; (*b*) total phase of three modes constituting one triplet for six different initial conditions; (*c*) amplitudes and (*d*) phases of all 15 modes for one initial condition (from [9]). Reproduced with permission from Wójcik et al., Opt. Eng. 2010, 49, 111114. Copyright (2010) by SPIE. (The color version of this figure is included in the online version of the journal.)

than in the case of the mean-field approximation because many interaction paths between the modes become forbidden. Nevertheless, simulations show that frequency and phase coupling is still possible.

Figure 5(*b*)–(*d*) shows the result of solving Equations (5) when each of the three lateral modes consists of five longitudinal modes, resulting in five triplets. The separation of the modes within each triplet is about two times smaller than the distance $\hbar c\pi/(n_{\mathrm{eff}}L_{\mathrm{c}}) \sim 0.1$ meV between neighboring longitudinal modes. In Figure 5(*b*) the dynamics of the total phases $\Theta_j(t)$ ($a_j \propto \exp[\mathrm{i}\Theta_j(t)]$) of three modes in a single triplet is shown for six randomly chosen initial conditions. Each mode is started from a random amplitude and phase. After the initial time of the order of the inverse growth rate of laser oscillations, frequencies of all three modes become locked to a single frequency independently on the initial conditions. Figure 5(*d*) demonstrates similar behavior for all five triplets. Moreover, we found that the evolution of modes constituting a single triplet is practically the same no matter how many triplets we included in the modeling. This allows us to consider in detail the dynamics of only one triplet.

The dynamics of the modes showed different regimes, depending on the gain. At lower gain values, the steady state was oscillatory, while at higher values the frequencies of the modes merged into a single frequency and steady state was achieved. This behavior is presented in Figure 6(*a*) and (*b*). The far field corresponding to the same simulations is shown in Figure 6(*c*), for completeness. The amplitude and frequencies of all *stable* steady state solutions of Equations (5) based on a large set of random initial conditions are presented in the same figure. For a given gain, we solve Equations (5) starting from a set of random initial conditions and identifying the steady states that were asymptotically approached by time-dependent solutions. The frequency of each mode in Figure 6 is defined as a derivative of the total phase; it is constant when the steady state is reached.

Simulations in Figure 6 reveal the existence of a certain critical current above which there is only one stable steady-state solution. A remarkable feature of this solution is that frequencies of all modes are locked to the same frequency. Below this critical current, there are multiple steady-state solutions with different uncorrelated frequencies and phases. This behavior

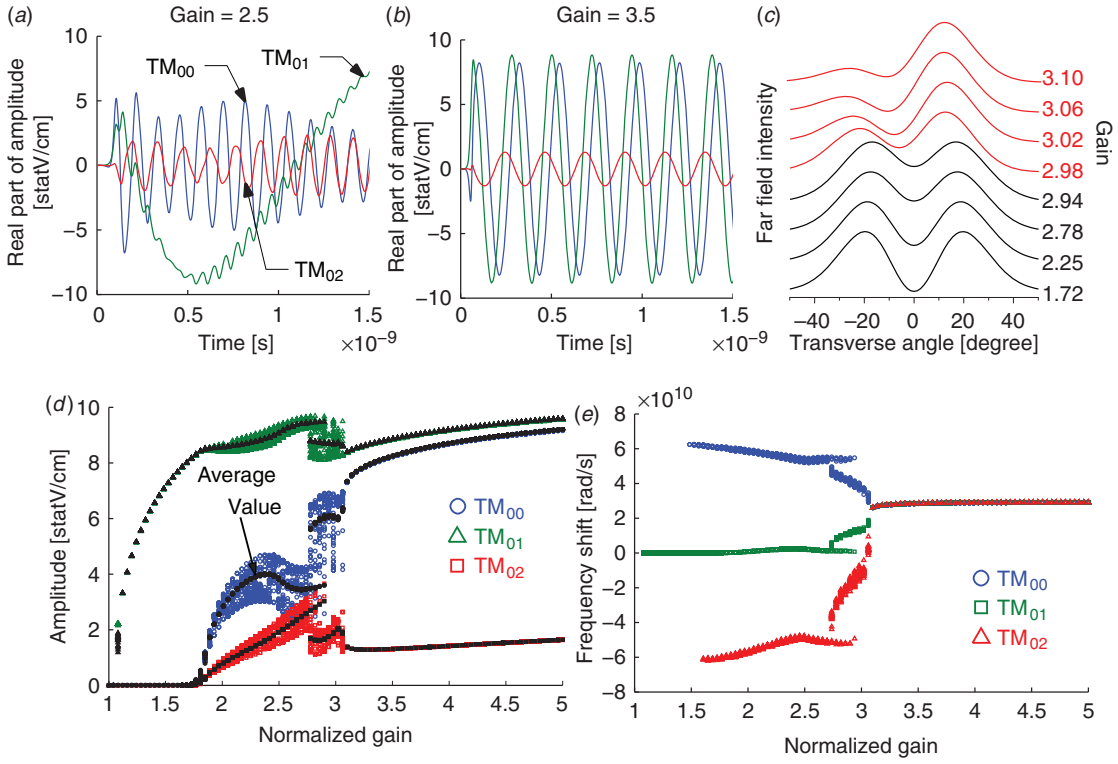

Figure 6. Time-dependent simulations for a single triplet of longitudinal modes. Time evolution of real parts of complex field amplitudes $a_i(t)$ for the linear normalized gain (*a*) 2.5 and (*b*) 3.5 times the laser threshold. (*c*) Normalized far-field distribution at different gains (curves are shifted for clarity). (*d*) Absolute values of the amplitudes and (*e*) frequencies of the modes as a function of the linear gain normalized to the threshold value, calculated for a large set of random initial conditions (from [8]). Reproduced with permission from Wójcik et al., Phys. Rev. Lett. 2011, 106, 133902. Copyright (2011) by the American Physical Society. (The color version of this figure is included in the online version of the journal.)

is in qualitative agreement with the experimental results under the mean-field approximation and those presented in Figure 3. Better agreement can be obtained by including interactions between different triplets (see [8]).

3. Mode locking and generation of ultrashort pulses

QCLs have tremendous technological potential and it would be highly desirable to operate them in the regime of ultrashort pulse generation. The QCL spectrum can be broad enough to support sub-picosecond pulses. Common mechanisms that destabilize continuous-wave (CW) generation and drive lasers into pulsed operation include gain or Q-switching, periodic external modulation of gain or loss, and the presence of an additional nonlinear element in the laser cavity (saturable absorber), which in effect provides self-modulation of both real and imaginary parts of net laser gain [35,36]. In the modal language, periodic (self-) modulation at frequency equal to intermode separation frequency or its multiple facilitates nonlinear coupling of frequencies and phases of longitudinal cavity modes (mode locking). The pulsed operation emerges when the spectral comb of longitudinal modes becomes equidistant and the EM field oscillations of modes are added with 'right' phases (zero phases).

Unfortunately, all of the above mechanisms of pulsed operation are facing a fundamental obstacle when applied to QCLs: ultrafast gain recovery dynamics. The measured gain relaxation time in QCLs utilizing a strong vertical laser transition is of the order of 1 ps [10], which is much shorter than the cavity roundtrip time (~50 ps in a few mm-long devices) and the photon lifetime (~10 ps). This unique feature enables ultrafast modulation of QCLs since it eliminates the relaxation oscillation peak in the high-frequency response [37,38]. At the same time, ultrafast build-up of laser field in the cavity makes gain or Q-switching methods of pulsed operation ineffective since it prevents accumulation of the EM field energy in the pulse. Recently demonstrated gain switching in terahertz QCLs required a sophisticated scheme implementing sub-picosecond turn-on of laser gain through the use of a femtosecond laser and an integrated Auston switch [39].

The situation is even worse with pulsed generation schemes that utilize CW pumping and periodic modulation of laser parameters. Here the analysis based on rate equations shows that to achieve stable single-pulse operation the gain should remain saturated by the pulse and stay below CW lasing threshold during the time the pulse traverses the cavity. It is impossible to achieve single-pulse operation through active or passive mode locking if the gain recovers from its saturated value to a small-signal value much faster than the cavity round-trip time. Although locking of cavity modes to equidistant frequencies and constant mutual phases is still possible under these conditions, the modes are locked to 'wrong' phases which correspond to a random output rather than isolated pulses. In the pioneering work [40] a sharp peak in the microwave spectrum at the cavity round-trip frequency was observed, which indicated the presence of coherent self-pulsations at the intermodal beat frequency, or, in other words, phase coherence between longitudinal modes that existed over the timescale of many thousand round-trip times. It was argued that self-mode locking was achieved due to the presence of saturable absorption mediated by the resonant Kerr effect in the active laser medium: the radiation spectrum was concentrated on the blue side of the gain resonance where the intensity dependent contribution to the refractive index was positive. As a result, the transverse mode experienced focusing to the waveguide axis with increasing intensity, and therefore its losses due to overlap with metal waveguide walls decreased. However, no pulse measurements were attempted in that work.

Frequency and phase locking between combs of longitudinal modes belonging to different lateral modes has been achieved in recent work reviewed in Section 2. Although there was no attempt to make time-resolved measurements in those experiments as well, numerical modeling indicated that phase coherence did not lead to formation of isolated pulses. Instead, simulated lasers either showed quasi-CW output originated from addition of many sinusoidal oscillations with different phases, or randomly switched between several steady states.

A breakthrough in QCL mode locking has been reported in [13,41]. In that work, a specially designed QCL with a 'superdiagonal' transition between widely separated electron states was employed. The upper state lifetime was of the order of 50 ps, i.e. comparable to the round-trip time. Although the gain recovery dynamics still had fast timescales related to the lower state depopulation and transport across the injector, the presence of a long timescale facilitated mode locking. Furthermore, the injection current was modulated at a frequency resonant to the cavity round-trip

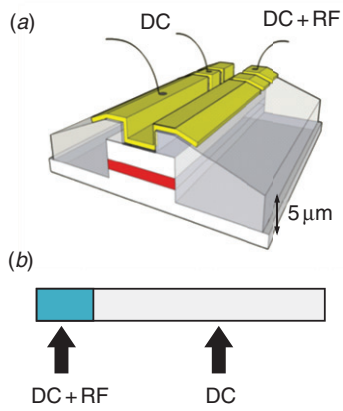

Figure 7. Configuration of the actively mode locked QCL (from [13]). (*a*) The geometry of the actively mode locked laser. (*b*) Both RF and DC components of the current are applied to the short section. In the longer section only the DC current is applied. Reproduced with permission from Wang et al., Opt. Express 2009, 17, 12929. Copyright (2009) by the Optical Society of America. (The color version of this figure is included in the online version of the journal.)

frequency only over the short section of the laser cavity, as shown in Figure 7.

Isolated mode-locked pulses of 3 ps duration were measured by interferometric autocorrelation technique when the laser was pumped just above threshold. With increasing CW component of the injection current, the pulses disappear because the RF modulation is not capable of keeping the gain below threshold. This work underscores difficulties in achieving robust active mode locking, while passive mode locking still remains a challenge.

A possible way to achieve ultrashort pulse operation in QCLs with fast gain recovery is to utilize coherent mechanisms of mode locking which go beyond rate equation approximation and do not rely on the saturation nonlinearity. This happens when the timescales of coherent interaction processes between laser light and active medium become shorter than the dephasing time T_2 of the optical polarisation. Such timescales may include the pulse duration, the build-up time of laser oscillations, or the period of Rabi oscillations of the population inversion and laser intensity. Because of a large matrix element of the intersubband laser transition this may actually happen at modest intracavity intensities easily reachable in QCLs.

An interesting theoretical and practical question is whether QCLs can be self-mode locked if the interaction of the radiation pulse with active medium and saturable absorber is coherent, i.e. the pulse duration is much shorter than the dephasing time of the optical polarisation at both amplifying and absorbing transition. Coherent pulse propagation in two-component media has been studied for over 40 years.

Numerical simulations reviewed in [42] show that an isolated stationary pulse can be formed and the shortest duration is reached under the conditions of self-induced transparency (SIT) [43], i.e. when the pulse area corresponds to a π-pulse in the amplifying medium and a 2π-pulse in the absorbing medium. A stationary pulse could also form when only the interaction with an amplifying medium is coherent; however, in this case its shape will be asymmetric and complicated.

The possibility of stable passive mode locking in lasers with saturable absorber under SIT conditions has been shown theoretically by Kozlov [44]. In the recent paper [16] these ideas were applied to QCLs and the specific QCL design implementing SIT conditions in both amplifying and absorbing parts of the laser has been proposed. A nice feature of this approach is that it requires that the gain relaxation time T_1 be much shorter than the cavity round-trip time, i.e. fast gain relaxation inherent to QCLs is an advantage rather than an obstacle in this case. Unfortunately, numerical simulations presented in [16] show that the laser in such a SIT mode-locked regime does not self-start: it requires seeding with pulses shorter than T_1 with area larger than approximately π. For typical QCL parameters this implies seeding with pulses of ≤ 1 ps duration and intensity at the level of at least a few MW cm^{-2}.

Another intriguing possibility to achieve passive mode locking under self-starting conditions in multimode lasers is to utilize the RNGH instability, named after the initials of the authors who predicted it in the late 1960s: Risken and Nummedal [45] and independently Graham and Haken [46]. The origin of this phenomenon is the oscillation of the population inversion at the Rabi frequency Ω_{Rabi} in the coherent regime, i.e. faster than $(T_1 T_2)^{1/2}$, which takes place when the intracavity laser intensity becomes sufficiently large. This results in a nonlinear deformation of the gain spectrum and the emergence of sidebands separated from the maximum of the small-signal gain curve by an amount corresponding to the Rabi frequency. These sidebands can be regarded as a manifestation of parametric instability of the central mode tuned to the peak of the small-signal gain. The process is sometimes called the second laser threshold as opposed to the first threshold corresponding to the onset of lasing. The small-signal gain corresponding to the second threshold is at least nine times higher than the first threshold. A similar destabilising mechanism with the same threshold operates in single-mode homogeneously broadened lasers [47], where, however, an additional requirement has to be fulfilled: the photon lifetime in a cavity must be shorter than the dephasing time T_2. In other words, the gain linewidth should fit within the cavity linewidth; see [11] for review.

Although the RNGH instability was predicted more than 40 years ago, its experimental demonstration remained debatable for decades [48–53].

The lack of an unambiguous experimental observation can be explained essentially by two reasons. First, the laser must be pumped approximately nine times above the lasing threshold for the RNGH instability to be observed [45,46]. This result, which can be established analytically, suggests that other nonlinearities or instabilities kick in before the RNGH mechanism becomes relevant. The second reason is the fact that for many lasers, the Rabi frequency is usually smaller than or comparable to the separation between adjacent longitudinal cavity modes. In other words, there are no modes within the unstable region of the spectrum.

If the RNGH instability does develop, it may lead to the multimode generation of frequency- and phase-locked modes. In [54] this mechanism was invoked to explain apparent self-mode locking in a ring fiber laser [50], which is a class-B laser with slow relaxation of inversion. The coupling occurs through parametric resonance between Rabi oscillations and the beatnote frequency of adjacent cavity modes. It was not entirely clear, however, how to explain the fact that in experiments the mode locking started at pumpings much lower than nine times the first laser threshold. In class-B lasers the presence of even weak saturable absorption can initiate conventional mode locking before the RNGH instability has a chance to develop.

In recent papers [14,15] the unambiguous observation of the RNGH instability was reported in different kinds of QCLs. It was shown that class-A lasers such as QCLs are ideal candidates for observing the RNGH instability because the conventional mechanism of instability of the CW operation based on saturable absorption is strongly suppressed by ultrafast gain relaxation. Moreover, it was found that the presence of a saturable absorber dramatically lowers the threshold of the RNGH instability, so that it can start almost immediately after the first laser threshold. Figure 8 shows one example of measured spectra which clearly shows generation of sidebands separated by twice the Rabi frequency. The waveguide was only 3 μm wide; therefore any nonlinear phase coupling mechanism related to interaction of multiple lateral modes is ruled out.

The surprising feature of the laser shown in Figure 8 and other lasers studied in [14,15] is a low instability threshold. For the laser in Figure 8 the current at the RNGH threshold is only 1.2 times higher than the current at the first laser threshold. One possible explanation is the presence of saturable

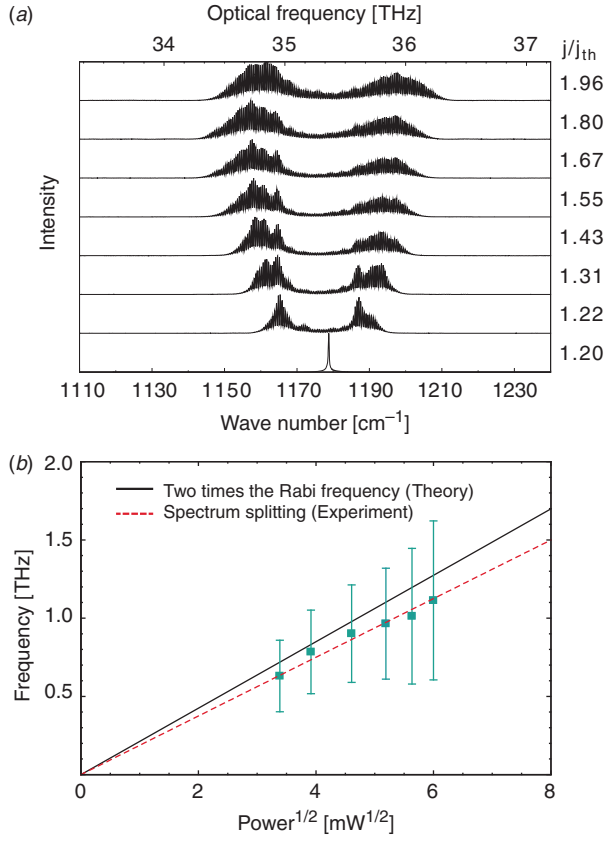

Figure 8. (*a*) Optical spectra versus injection current in CW regime at 300 K with a 3 μm-wide buried heterostructure laser emitting at 8.47 μm. (*b*) Spectral splitting and twice the Rabi frequency $_{\text{Rabi}}/2\pi$ versus square root of output power collected from a single laser facet. The different quantities reported on the graph were deduced from the experimental data shown in (*a*). The dashed line is a least-squares linear fit of the data (from [14]). Reproduced with permission from Wang et al. Phys. Rev. A 2007, 75, 031802. Copyright (2007) by the American Physical Society. (The color version of this figure is included in the online version of the journal.)

absorption due to the Kerr effect, similar to the devices studied in [40]. This suggestion is supported by the fact that the RNGH instability is observed only in lasers with narrow waveguides.

Below we derive some analytical results illustrating the main features of the RNGH instability. For simplicity we present the results for laser radiation propagating in one direction (a ring cavity laser), neglecting the grating of population inversion formed by counter-propagating waves in a Fabry–Pérot cavity. This neglects the effect of spatial hole burning (SHB) which also leads to a multimode generation and which is actually quite important in QCLs. In [15] both RNGH and SHB instabilities are included and it is shown that they can be analysed independently. The treatment of the RNGH instability of unidirectional waves presented below is slightly more general than in [15] because here we do not assume that the steady state solution is constant in space and perturbations are plane waves along the cavity.

Since we are interested in the coherent and ultrafast processes, the polarisation and inversion of the gain medium cannot be adiabatically eliminated. Therefore, we start from the full set of Maxwell–Bloch equations in a two-level medium for slow amplitudes and in dimensionless form, in which we split complex amplitudes of the field and polarization into real amplitudes and phases. We will generally follow the technique described in [55].

$$\frac{\partial e}{\partial z}+\frac{\partial e}{\partial t}=2f\left(p\sin\Phi-\frac{1}{2}\eta e-\frac{1}{2}\frac{qe}{1+(e^2/I_{\text{a}})}\right), \tag{12}$$

$$e\frac{\partial\varphi}{\partial z}+e\frac{\partial\varphi}{\partial t}=-2fp\cos\Phi, \tag{13}$$

$$\frac{\partial p}{\partial t}=g[(1/2)ne\sin\Phi-p], \tag{14}$$

$$p\frac{\partial\psi}{\partial t}=\Delta p+(1/2)\,gne\cos\Phi, \tag{15}$$

$$\frac{\partial n}{\partial t}=d-n-2pe\sin\Phi, \tag{16}$$

$$e(0,t)=R_1R_2e(2L,t),\quad \varphi(0,t)=\varphi(2L,t). \tag{17}$$

Here n is the normalized inversion, d is the inversion supported by pumping in the absence of generation; slow amplitudes of the electric field and polarisation are suitably normalized and defined as

$$E=\frac{1}{2}e\exp[\mathrm{i}(\omega t-kz+\varphi)]+\text{c.c.},$$
$$P=\frac{1}{2}p\exp[\mathrm{i}(\omega t-kz+\varphi)]+\text{c.c.} \tag{18}$$

The electric field is normalized according to $e'=\mu e\sqrt{T_1T_2}/\hbar$, where μ is the dipole moment of the gain transition, and all dependent variables and parameters are made dimensionless using T_1 and v, where v is the phase velocity of a given waveguide mode. For example $t'=t/T_1$, $z'=z/(vT_1)$, and all primes are dropped in the above equations. Other parameters introduced above are $\Delta=T_1(\omega-\omega_{\text{a}})$, where ω_{a} is the central frequency of the gain spectrum, $f=T_1/T_{\text{p}}$, $g=T_1/T_2$, $\eta=\alpha_{\text{w}}/\alpha_t$, $q=\alpha_{\text{a}}/\alpha_t$, T_{p} the photon lifetime in a cavity, α_{w} the waveguide losses, α_{a} the unsaturated losses due to absorber, I_{a} the saturation intensity of the absorber, $\alpha_t=\alpha_{\text{w}}+\alpha_{\text{a}}+(1/L)\ln[1/(R_1R_2)]=1/(vT_{\text{p}})$ the total small-signal losses, L the cavity length, $R_{1,2}$ the amplitude reflection factors of the cavity mirrors. Unless specified

otherwise, in all plots below we assume $T_1 = 2\,\text{ps}$, $T_2 = 0.05\,\text{ps}$, $T_p = 5\,\text{ps}$, $L = 2\,\text{mm}$, $I_a = 2$.

We will assume the field to be split in a set of longitudinal modes: $\omega_j = \omega + 2\pi j/T$, where $T = 2L/v$ is the round-trip time in a cavity, j is integer.

Consider for simplicity the stability of the jth mode with zero normalized detuning $\Delta_j = 0$, i.e. the mode tuned to the center of the gain spectrum. For this mode the stability for the amplitude and phase variables can be studied separately, because in the steady state $\cos\Phi = 0$, i.e. there is $\pi/2$ shift between the CW field and polarisation. Consider amplitude equations in Equations (12), (14) and (16). First, we find the non-trivial steady state solution (denoted with a bar below) corresponding to a stable CW generation by dropping all time derivatives and solving the resulting differential equations with respect to z. We write $e = \bar{e} + \tilde{e}$ and the same for p and n. Then we linearize with respect to variables with tilde and take the Laplace transform

$$e(z,s) = \int_0^\infty \tilde{e}(z,t)\exp(-st)\,\mathrm{d}t$$

and the same for p and n, and finally obtain for Laplace transforms $e(z,s)$, $p(z,s)$, and $n(z,s)$:

$$\frac{\partial e}{\partial z} + se = 2f\left(p - \frac{1}{2}\eta e - \frac{1}{2}\frac{qe\left(1-\frac{\bar{e}^2}{I_a}\right)}{\left(1+\frac{\bar{e}^2}{I_a}\right)^2}\right) + e(z,t=0), \tag{19}$$

$$sp = \frac{1}{2}(g\bar{k}e + gk\bar{e} - gp + p(z,t=0), \tag{20}$$

$$sn = -n - 2\bar{p}e - 2p\bar{e} + n(z,t=0). \tag{21}$$

Then we eliminate p and n in Equations (19)–(21) and solve the resulting differential equation for $e(z,s)$. Of course we cannot completely integrate it because barred variables are integrals over z themselves. However, we do not need the answer fully integrated. Instead, we notice that using the boundary condition the solution for the Laplace transform $e(2L,s)$ can be written as the ratio of two quasi-polynomials:

$$e(2L,s) = \frac{\Gamma(2L,s)}{\Sigma(2L,s)}, \tag{22}$$

where $\Gamma(2L,s)$ contains complicated integrals over initial distributions of e, p, and n that we do not need to know, while

$$\Sigma(2L,s) = 1 - R_1R_2\exp\left(-\int_0^{2L} F(z)\,\mathrm{d}z\right), \tag{23}$$

where

$$F(z) = s + f\eta + fq\frac{\left(1-(\bar{e}^2/I_a)\right)}{\left(1+(\bar{e}^2/I_a)\right)^2} + \frac{2fg(s+1)}{(s+g)(s+1)+g\bar{e}^2}\left[\frac{\bar{p}\bar{e}}{s+1} - \frac{\bar{n}}{2}\right]. \tag{24}$$

Taking the inverse Laplace transform and closing the integration loop in the complex s-plane in the appropriate way allows us to write

$$\tilde{e}(2L,t) = \frac{1}{2\pi\mathrm{i}}\oint e(2L,s)\exp(st)\,\mathrm{d}s = \sum_{i=-\infty}^{\infty} C_i\exp(s_it), \tag{25}$$

where s_i are roots of the quasi-polynomial $\Sigma(2L,s)$ that determine the residues of the integrand in Equation (25). If at least one of them has a positive real part, this means instability of CW generation. After some manipulation, using steady-state (barred) solutions for e, p, and n in the expression for $F(z)$, we find that the eigenvalues s_i should be the roots of the characteristic equation

$$s^3 + s^2\left(1 + f + g + \mathrm{i}\Omega_m - \frac{fq(d-1)}{I_a + d - 1}\right) + s\left(f + dg + \mathrm{i}\Omega_m(g+1) - \frac{fq(d-1)(g+1)}{I_a + d - 1)}\right) + 2fg(d-1) + \mathrm{i}\Omega_m dg - \frac{fqg(d-1)^2}{I_a + d - 1} = 0. \tag{26}$$

Here $\Omega_m = 2\pi m T_1/T$ and m is integer. Equation (26) is the main result of the linear stability analysis. It can be easily analyzed on a computer and further simplified because we expect the solution of interest to have an imaginary part close to $-\mathrm{i}\Omega_m$. If we write this root as $s = -\mathrm{i}\Omega_m + x$ and linearise with respect to x, we obtain the analytic result for x:

$$x = \frac{\Omega_m^2(f-A) + \mathrm{i}\Omega_m(f - A(g+1)) - g(d-1)(2f-A)}{-\Omega_m^2 - \mathrm{i}\Omega_m(g+1+2(f-A)) + f + dg - A(g+1)}, \tag{27}$$

where $A = fq(d-1)/(I_a + d - 1)$ is a small parameter characterizing a saturable absorber. Real parts of the exact solution for s and approximate expression for x are very close to each other in the region of interest where the real part of s is greater than zero.

Figure 9 shows the spectrum of the RNGH instability, namely the instability growth rate normalized by T_1 (real part of x in Equation (27)) when the pumping is two times above threshold for two values of the normalized unsaturated losses in the absorber: $q = 0$ (dashed curve) and $q = 0.2$ (solid curve). The modal frequency along the horizontal axis is

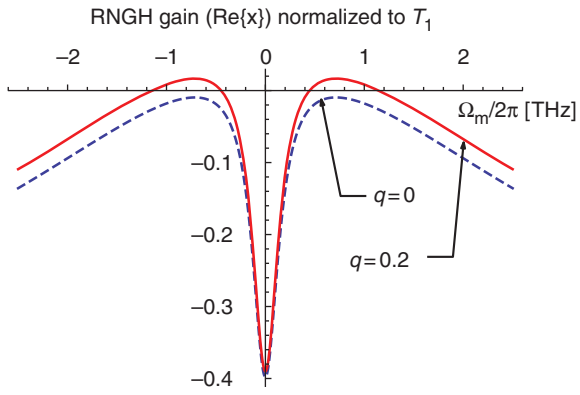

Figure 9. Growth rate of the RNGH instability, defined as a real part of x in Equation (27), as a function of the mode frequency for $d=2$ and two values of the normalized unsaturated losses in the absorber: $q=0$ (dashed curve) and $q=0.2$ (solid curve). The instability takes place where $\Re\{x\} > 0$. (The color version of this figure is included in the online version of the journal.)

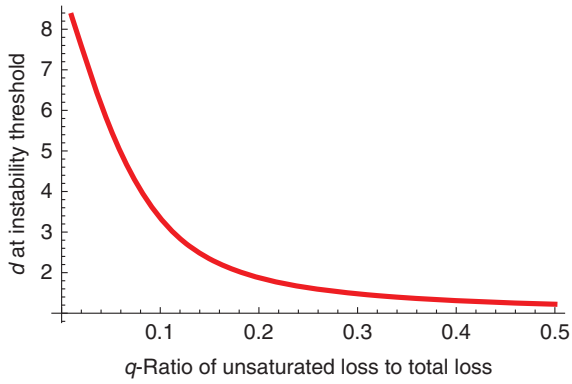

Figure 10. Pumping parameter d corresponding to RNGH instability threshold normalized to pumping at CW lasing threshold as a function of the unsaturated loss in the absorber q normalized to the total photon losses in the cavity. (The color version of this figure is included in the online version of the journal.)

converted back to dimensional units and expressed in THz.

The instability takes place where the real part of x is positive. The peak growth rate scales roughly as the Rabi frequency, which for a constant CW field amplitude and in the absence of a saturable absorber is equal to $\Omega_{\text{Rabi}} = [g(d-1)]^{1/2}$. The spectral boundaries of the instability regions are the solutions of the bi-quadratic equation

$$\Omega_m^4(1-A) - \Omega_m^2[g(d-1)(3-2A) + A(g^2+g+1) - 1] + g^2 d(d-1)(2-A) = 0. \quad (28)$$

The instability regions are symmetric with respect to $\Omega_m = 0$, so we will consider only positive frequencies. The bifurcation value of the frequency corresponding to the set of laser parameters when these two boundaries shrink to a single point is given by

$$\Omega_m^2 = \frac{\Omega_R^2(3-2A) + A(g^2+g+1) - 1}{2(1-A)}.$$

Laser parameters corresponding to this bifurcation (emergence of an instability) can be obtained by equating the determinant of Equation (28) to zero. For example, one can find the pumping parameter d needed to reach the instability threshold as a function of the unsaturated losses in the absorber q. The result is shown in Figure 10.

As is clear from the figure, with increasing losses in the absorber the pumping at the instability threshold approaches the first laser threshold of CW lasing. The threshold for the RNGH instability also decreases with increasing saturation intensity of the absorber and increasing ratio T_1/T_2 and T_1/T_p.

The above analytic theory describes only the linear stage of the instability. Laser dynamics at the nonlinear stage has been investigated numerically in [14,15] and compared with experiment. These studies have shown that the competing mechanism for the multimode operation based on the SHB in the Fabry–Pérot cavity plays an important role in QCLs and in many cases sets in before the RNGH instability becomes relevant. Moreover, the SHB mechanism appears to strongly affect laser spectra and phases of the modes even when the RNGH instability is prominent. Strong mode coupling via the SHB nonlinearity could be one reason why none of the lasers studied in [14,15] showed the formation of isolated pulses. The interferometric autocorrelation traces always indicated the random output. It could be interesting to explore the dynamics of QCLs fabricated in the shape of a ring cavity and check if the RNGH instability can lead to pulsed operation.

4. Conclusions

In conclusion, recent experimental and theoretical studies show that phase-sensitive nonlinear mixing of laser modes in mid-infrared QCLs is the universal phenomenon affecting the devices of various active region design and overall geometry. Factors that make nonlinear phase coupling so prominent and stable include giant saturation nonlinearity of the intersubband transitions which facilitates four-wave mixing interaction and Kerr nonlinearity, high Rabi frequency of the intracavity field which can be comparable to or

higher than the relaxation rates in the active medium, and ultrafast relaxation time of population inversion across the gain transition, which leads to overdamped relaxation oscillations.

A particularly interesting case of nonlinear mode mixing is realized in buried heterostructure QCLs with wide waveguides which are able to lase simultaneously on several transverse (lateral) modes with similar modal losses. At high enough radiation intensities, the nonlinear coupling between combs of longitudinal modes belonging to different lateral modes leads to frequency and phase locking of multiple lateral modes (three modes in the experiment). In some cases this locking results in a complete synchronization of lateral modes when three combs merge into a single comb whereas the far field pattern experiences a strong beam steering effect. Transverse mode locking originates from the four-wave mixing interaction with the saturation nonlinearity of the gain transition only, without any additional nonlinear element in the cavity or an external modulation.

The phase coupling of transverse modes can be affected and controlled by selective inhomogeneous current injection or by selective modulation of modal losses through the fabrication of the metallic structure on top of the laser waveguide. The resulting phase locked multimode spectrum could be further utilized for creating stable mid-infrared frequency combs and various far-field radiation patterns, controlling the beam quality and beam steering, or facilitating ultrashort pulse generation.

Narrow waveguide QCLs which support only one transverse mode demonstrate a peculiar coherent mechanism of the nonlinear phase locking of longitudinal modes associated with the RNGH instability. In fact, QCLs seem to constitute the first unambiguous case of observation of this instability because of the absence of the competing conventional mode locking mechanism based on the saturable absorption nonlinearity. However, in all experiments so far the RNGH-based mechanism of mode coupling did not lead to generation of isolated ultrashort pulses. The only demonstrated way to obtain mode-locked pulse generation at the cavity round-trip frequency is through the active mode locking, namely an RF modulation of the current through a short section of the QCL. Pulsed operation is inhibited by ultrafast gain relaxation and by the pervasive multimode instability associated with the spatial hole burning which seems to be present in virtually all studies of multimode dynamics of QCLs. It remains to be seen whether these challenges can be overcome and ultrashort pulse generation through passive mode locking becomes possible.

Acknowledgements

This work was supported in part by NSF Grants ECS-0547019 (CAREER) and EEC-0540832 (MIRTHE ERC).

References

[1] Lyakh, A.; Maulini, R.; Tsekoun, A.; Go, R.; Von der Porten, S.; Pflugl, C.; Diehl, L.; Capasso, F.; Patel, C.K.N. *Proc. Natl. Acad. Sci. USA* **2010,** *107,* 18799–18802.

[2] Gokden, B.; Bai, Y.; Bandyopadhyay, N.; Slivken, S.; Razeghi, M. *Appl. Phys. Lett.* **2010,** *97,* 131112.

[3] Bai, Y.; Slivken, S.; Darvish, S.R.; Haddadi, A.; Gokden, B.; Razeghi, M. *Appl. Phys. Lett.* **2009,** *95,* 221104.

[4] Liu, P.Q.; Hoffman, A.J.; Escarra, M.D.; Franz, K.J.; Khurgin, J.B.; Dikmelik, Y.; Wang, X.J.; Fan, J.Y.; Gmachl, C.F. *Nat. Photonics* **2010,** *4,* 95–98.

[5] Belkin, M.A.; Capasso, F.; Xie, F.; Belyanin, A.; Fischer, M.; Wittman, A.; Faist, J. *Appl. Phys. Lett.* **2008,** *92,* 201101.

[6] Kumar, S.; Chan, C.W.I.; Hu, Q.; Reno, J.L. *Nat. Phys.* **2011,** *7,* 166–171.

[7] Yu, N.; Diehl, L.; Cubukcu, E.; Bour, D.; Corzine, S.; Höfler, G.; Wojcik, A.K.; Crozier, K.B.; Belyanin, A.; Capasso, F. *Phys. Rev. Lett.* **2009,** *102,* 013901.

[8] Wójcik, A.K.; Yu, N.; Diehl, L.; Capasso, F.; Belyanin, A. *Phys. Rev. Lett.* **2001,** *106,* 133902.

[9] Wójcik, A.K.; Yu, N.; Diehl, L.; Capasso, F.; Belyanin, A. *Opt. Eng.* **2010,** *49,* 111114.

[10] Choi, H.; Norris, T.B.; Gresch, T.; Giovannini, M.; Faist, J.; Diehl, L.; Capasso, F. *Appl. Phys. Lett.* **2008,** *92,* 122114.

[11] Khanin, Y. *Principles of Laser Dynamics*; Elsevier: Amsterdam, 1995.

[12] Staliunas, K.; Tarroja, M.; Weiss, C. *Opt. Commun.* **1993,** *102,* 69–75.

[13] Wang, C.Y.; Kuznetsova, L.; Gkortsas, V.M.; Diehl, L.; Kärtner, F.X.; Belkin, M.A.; Belyanin, A.; Li, X.; Ham, D.; Schneider, H.; Grant, P.; Song, C.Y.; Haffouz, S.; Wasilewski, Z.R.; Liu, H.C.; Capasso, F. *Opt. Express* **2009,** *17,* 12929.

[14] Wang, C.; Diehl, L.; Gordon, A.; Jirauschek, C.; Kartner, F.X.; Belyanin, A.; Bour, D.; Corzine, S.; Haoer, G.; Troccoli, M.; Faist, J.; Capasso, F. *Phys. Rev. A Rapid Commun.* **2007,** *75,* 031802.

[15] Gordon, A.; Wang, C.; Diehl, L.; Kärtner, F.X.; Belyanin, A.; Bour, D.; Corzine, S.; Höfler, G.; Liu, H.C.; Schneider, H.; Maier, T.; Troccoli, M.; Faist, J.; Capasso, F. *Phys. Rev. A* **2008,** *77,* 053804.

[16] Menyuk, C.R.; Talukder, M.A. *Phys. Rev. Lett.* **2009,** *102,* 023903.

[17] Mandel, P.; Tlidi, M. *J. Opt. B: Quantum Semiclass. Opt.* **2004,** *6,* R60–R75.

[18] Schöll, E.; Schuster, H.G., Eds. *Handbook of Chaos Control*; Wiley-VCH: Weinheim, 2008.

[19] Otsuka, K.; Chu, S.-C.; Lin, C.-C.; Tokunaga, K.; Ohtomo, T. *Opt. Express* **2009,** *17,* 21615–21627.
[20] Wiesenfeld, K.; Peles, S.; Rogers, J. *IEEE J. Sel. Top. Quantum Electron.* **2009,** *15,* 312–319.
[21] Bewley, W.; Lindle, J.; Kim, C.S.; Vurgaftman, I.; Meyer, J.R.; Evans, A.J.; Yu, J.S.; Slivken, S.; Razeghi, M. *IEEE J. Quantum Electron.* **2005,** *41,* 833–841.
[22] Yu, N.; Blanchard, R.; Fan, J.; Wang, Q.J.; Pflugl, C.; Diehl, L.; Edamura, T.; Furuta, S.; Yamanishi, M.; Kan, H.; Capasso, F. *IEEE Trans. Nanotechnol.* **2010,** *9,* 11–29.
[23] Hoffmann, L.K.; Hurni, C.A.; Schartner, S.; Mujagić, E.; Andrews, A.M.; Klang, P.; Schrenk, W.; Semtsiv, M.P.; Masselink, W.T.; Strasser, G. *Appl. Phys. Lett.* **2008,** *92,* 061110.
[24] Allen, D.; Hargett, T.W.; Reno, J.; Wanke, M.C. *IEEE J. Sel. Top. Quantum Electron.* **2011,** *17,* 222–228.
[25] Fathololoumi, S.; Dupont, E.; Razavipour, S.G.; Laframboise, S.R.; Delage, A.; Wasilewski, Z.R.; Bezinger, A.; Rafi, G.Z.; Safavi-Naeini, S.; Ban, D.; Liu, H.C. *Opt. Express* **2010,** *18,* 10036–10048.
[26] Indjin, D.; Harrison, P.; Kelsall, R.W.; Ikonic, Z. *J. Appl. Phys.* **2002,** *91,* 9019.
[27] Nelander, R.; Wacker, A.; Pereira Jr, M.F.; Revin, D.G.; Soulby, M.R.; Wilson, L.R.; Cockburn, J.W.; Krysa, A.B.; Roberts, J.S.; Airey, R.J. *J. Appl. Phys.* **2007,** *102,* 113104.
[28] Hofstetter, D.; Beck, M.; Aellen, T.; Faist, J.; Oesterle, U.; Ilegems, M.; Gini, E.; Melchior, H. *Appl. Phys. Lett.* **2001,** *78,* 1964–1966.
[29] Rana, F.; Ram, R.J. *Phys. Rev. B* **2002,** *65,* 125313.
[30] Gensty, T.; Elsäβer, W.; Mann, C. *Opt. Express* **2005,** *13,* 2032–2039.
[31] Yu, N.; Diehl, L.; Cubukcu, E.; Pflugl, C.; David, B.; Scott, C.; Zhu, J.; Hofler, G.; Crozier, K.B.; Capasso, F. *Opt. Express* **2007,** *15,* 13227–13235.
[32] Hinkov, B.; Fuchs, F.; Bronner, W.; Kohler, K.; Wagner, J. *IEEE J. Quantum Electron.* **2008,** *44,* 1124–1128.
[33] Wang, Q.J.; Pflugl, C.; Diehl, L.; Capasso, F.; Edamura, T.; Furuta, S.; Yamanishi, M.; Kan, H. *Appl. Phys. Lett.* **2009,** *94,* 011103.
[34] Stelmakh, N.; Vasilyev, M.; Toor, F.; Gmachi, C. *Appl. Phys. Lett.* **2009,** *94,* 013501.
[35] Yariv, A. *Quantum Electronics*; Wiley: New York, 1989.
[36] Haus, H.A. *IEEE J. Sel. Top. Quantum Electron.* **2000,** *6,* 1173–1185.
[37] Capasso, F.; Paiella, R.; Martini, R.; Colombelli, R.; Gmachl, C.; Myers, T.L.; Taubman, M.S.; Williams, R.M.; Bethea, C.G.; Unterrainer, K.; Hwang, H.Y.; Sivco, D.L.; Cho, A.Y.; Sergent, A.M.; Liu, H.C.; Whittaker, E.A. *IEEE J. Quantum Electron.* **2002,** *38,* 511–532.
[38] Chen, G.; Bethea, C.G.; Martini, R.; Grant, P.D.; Dudek, R.; Liu, H.C. *Appl. Phys. Lett.* **2009,** *95,* 101104.
[39] Jukam, N.; Dhillon, S.S.; Oustinov, D.; Madeo, J.; Manquest, C.; Barbieri, S.; Sirtori, C.; Khanna, S.P.; Linfield, E.H.; Davies, A.G.; Tignon, J. *Nat. Photonics* **2009,** *3,* 715–719.
[40] Paiella, R.; Capasso, F.; Gmachl, C.; Sivco, D.L.; Baillargeon, J.N.; Hutchinson, A.L.; Cho, A.Y.; Liu, H.C. *Science* **2000,** *290,* 1741–1744.
[41] Gkortsas, V.-M.; Wang, C.; Kuznetsova, L.; Diehl, L.; Gordon, A.; Jirauschek, C.; Belkin, M.A.; Belyanin, A.; Capasso, F.; Kärtner, F.X. *Opt. Express* **2010,** *18,* 13616–13630.
[42] Kryukov, P.; Letokhov, V. *Usp. Fiz. Nauk* **1969**, *99*, 169–247, in Russian [*Sov. Phys. Usp.* **1970**, *12*, 641–672].
[43] Allen, L.; Eberly, J.H. *Optical Resonance and Two Level Atoms*; Dover: New York, 1987.
[44] Kozlov, V. *Phys. Rev. A* **1997,** *56,* 1607–1612.
[45] Risken, H.; Nummedal, K. *J. Appl. Phys.* **1968,** *39,* 4662–4672.
[46] Graham, P.; Haken, H. *Z. Phys.* **1968,** *213,* 420–450.
[47] Grasiuk, A.Z.; Oraevsky, A.N. Transient Processes in a Beam Maser. In *Proceedings of the VI International Congress on Microwave Tubes*; Centrex Publishing: Scheveningen, Holland, 1962.
[48] Hillman, L.W.; Krasiński, J.; Boyd, R.W.; Stroud, C.R. *Phys. Rev. Lett.* **1984,** *52,* 1605–1608.
[49] Hogenboom, E.H.M.; Klische, W.; Weiss, C.O.; Godone, A. *Phys. Rev. Lett.* **1985,** *55,* 2571–2574.
[50] Pessina, E.M.; Bonfrate, G.; Fontana, F.; Lugiato, L.A. *Phys. Rev. A* **1997,** *56,* 4086–4093.
[51] Voigt, T.; Lenz, M.; Mitschke, F.; Roldan, E.; De Valearcel, G.J. *Appl. Phys. B* **2004,** *79,* 175–183.
[52] Fu, H.; Haken, H. *J. Opt. Soc. Am. B* **1988,** *5,* 899–908.
[53] Roldán, E.; de Valcárcel, G.J.; Urchueguia, J.F.; Guerra, K.M. *J. Opt. Soc. Am. B* **2003,** *20,* 816–824.
[54] Kocharovsky, V.; Kocharovsky, Vl. *Radiophys. Quantum Electron.* **2001,** *44,* 443–447.
[55] Samson, A.; Kotomtseva, L.; Loiko, N. *Oscillations in Lasers*; Nauka i Tekhnika: Minsk, 1990 (in Russian).